



Super Plastic Bulk Metallic Glasses at Room Temperature

Yan Hui Liu, *et al.*

Science **315**, 1385 (2007);

DOI: 10.1126/science.1136726

The following resources related to this article are available online at www.sciencemag.org (this information is current as of March 8, 2007):

Updated information and services, including high-resolution figures, can be found in the online version of this article at:

<http://www.sciencemag.org/cgi/content/full/315/5817/1385>

Supporting Online Material can be found at:

<http://www.sciencemag.org/cgi/content/full/315/5817/1385/DC1>

This article **cites 10 articles**, 3 of which can be accessed for free:

<http://www.sciencemag.org/cgi/content/full/315/5817/1385#otherarticles>

This article appears in the following **subject collections**:

Materials Science

http://www.sciencemag.org/cgi/collection/mat_sci

Information about obtaining **reprints** of this article or about obtaining **permission to reproduce this article** in whole or in part can be found at:

<http://www.sciencemag.org/about/permissions.dtl>

33. S. A. Kivelson, E. Fradkin, V. J. Emery, *Nature* **393**, 550 (1998).
34. S. E. Brown, E. Fradkin, S. A. Kivelson, *Phys. Rev. B* **71**, 224512 (2005).
35. Y. Chen, T. M. Rice, F. C. Zhang, *Phys. Rev. Lett.* **97**, 237004 (2006).
36. L. Capriotti, D. J. Scalapino, R. D. Sedgewick, *Phys. Rev. B* **68**, 014508 (2003).
37. N. Read, S. Sachdev, *Phys. Rev. Lett.* **62**, 1694 (1989).
38. J. Zaanen, O. Gunnarsson, *Phys. Rev. B* **40**, 7391 (1989).
39. S. R. White, D. J. Scalapino, *Phys. Rev. Lett.* **80**, 1272 (1998).
40. V. J. Emery, S. A. Kivelson, J. M. Tranquada, *Proc. Natl. Acad. Sci. U.S.A.* **96**, 8814 (1999).
41. S. Sachdev, *Rev. Mod. Phys.* **75**, 913 (2003).
42. J. M. Tranquada, B. J. Sternlieb, J. D. Axe, Y. Nakamura, S. Uchida, *Nature* **375**, 561 (1995).
43. J. M. Tranquada *et al.*, *Nature* **429**, 534 (2004).
44. P. Abbamonte *et al.*, *Nat. Phys.* **1**, 155 (2005).
45. Ş. Smađići *et al.*, *Phys. Rev. B* **75**, 075104 (2007).
46. We acknowledge and thank P. Abbamonte, P. W. Anderson, E. Dagotto, S. A. Kivelson, D.-H. Lee, A. P. Mackenzie, N. P. Ong, M. Randeria, T. M. Rice, S. Sachdev, A. Sandvik, G. A. Sawatzky, D. J. Scalapino, J. M. Tranquada, N. Trivedi, S. R. White, Y. J. Uemura, J. Zaanen, and F. C. Zhang for helpful conversations and communications. This work was supported by the U.S. Department of Energy, Office of Naval Research, Natural Sciences and Engineering Research Council of Canada, Grants-in-Aid for Scientific Research from the Ministry of

Science and Education (Japan), and the 21st-Century Centers of Excellence Program for the Japan Society for the Promotion of Science. Fellowship support is acknowledged by K.F. from I²CAM and by A.S. from the Army Research Office.

Supporting Online Material

www.sciencemag.org/cgi/content/full/1138584/DC1

SOM Text

Figs. S1 to S3

References

8 December 2006; accepted 26 January 2007

Published online 8 February 2007;

10.1126/science.1138584

Include this information when citing this paper.

REPORTS

Super Plastic Bulk Metallic Glasses at Room Temperature

Yan Hui Liu, Gang Wang, Ru Ju Wang, De Qian Zhao, Ming Xiang Pan, Wei Hua Wang*

In contrast to the poor plasticity that is usually observed in bulk metallic glasses, super plasticity is achieved at room temperature in ZrCuNiAl synthesized through the appropriate choice of its composition by controlling elastic moduli. Microstructures analysis indicates that the super plastic bulk metallic glasses are composed of hard regions surrounded by soft regions, which enable the glasses to undergo true strain of more than 160%. This finding is suggestive of a solution to the problem of brittleness in, and has implications for understanding the deformation mechanism of, metallic glasses.

High strength has been a long-standing objective pursued in metals and alloys and was often achieved through the reduction of grain size (1). However, with increasing strength, plasticity is normally reduced. This trend has persisted in nanocrystalline metals and alloys, which display highly improved strength but very little plastic deformation (2), and in bulk metallic glasses (BMGs) with completely disordered atomic structures. BMGs have strengths approaching the theoretical limit (~Young's modulus $E/10$) (3), but their plasticity at room temperature is very low. In uniaxial tension, the plastic strain is near zero (4). Even under compression, the plastic strain still remains very limited (<2%), resulting from shear localization and work softening. Lack of plasticity makes BMGs prone to catastrophic failure in load-bearing conditions and restricts their widespread application. This also hinders precise study on some fundamental issues in glasses, such as the deformation mechanism and the dynamics of plastic deformation, in which large plasticity is needed for detailed analysis (5).

Plastic deformation of metallic glasses at room temperature occurs through the formation

and evolution of shear bands and is localized in thin shear bands. Therefore, brittleness is regarded as an intrinsic defect of metallic glasses. Efforts have been made to enhance the plasticity of BMGs, but most focus on the fabrication of BMG composites (6–9). It is expected that the

formation of multiple shear bands throughout a sample is needed for improving its plasticity, because each band contributes to the plasticity and none carry enough deformation to cause catastrophic failure (10). By careful selection of their compositions, several BMGs have been found to exhibit substantially increased plasticity (4, 6, 9). However, the hypotheses have not been fully verified, and methods for controlling the formation and evolution of shear bands in BMGs to improve their plasticity is a remaining challenge.

It was recently found that the toughness of BMGs correlates with Poisson's ratio ν (11). A large ν is regarded as an indicator of the plastic character of a BMG and could therefore be used as a means of identifying plastic BMGs (9). This idea was verified in a ductile Pt-based BMG (9) and in brittle Mg-based BMGs (12), as well as in Fe-based BMGs that display crossover from brittle to ductile behavior via the control of ν (13). Furthermore, it was also found that elastic

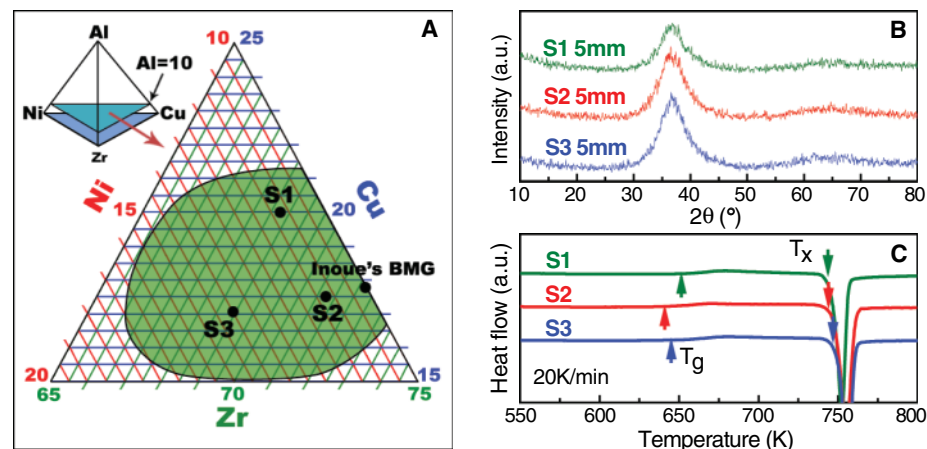


Fig. 1. (A) A family of quaternary ZrCuNiAl BMGs is obtained in the composition range (green area). In three compositions (circles labeled S1 to S3), ν is larger relative to that of other compositions (the values for ν of the ZrCuNiAl BMGs with poor plasticity are normally around 0.365). The representative Inoue's BMG is included for comparison. (B) XRD patterns of the BMGs in the form of 5-mm rods show no crystals. θ , XRD scattering angle; a.u., arbitrary units. (C) DSC curves exhibit distinct glass transition and crystallization, confirming the glassy nature of the as-cast super plastic BMGs (the heating rate is 20 K/min).

Institute of Physics, Chinese Academy of Sciences, Beijing 100080, China.

*To whom correspondence should be addressed. E-mail: whw@aphy.iphy.ac.cn

constants of metallic glasses scale with the weighted averages of those of their components (14). Therefore, the elastic moduli provide useful guidelines for the development of plastic BMGs with large ν by the appropriate choice of their composition.

In this study, a family of BMGs consisting of conventional metallic components Zr, Cu, Ni, and Al was obtained. Through compositional changes, we created BMGs that have relative large ν values and display an ability to undergo superplasticity-like deformation behavior at room temperature. The exceptional deformability is ascribed to the homogeneous and concurrent nucleation and evolution of high-density shear bands throughout the samples, which are composed of hard regions surrounded by soft regions.

The BMGs were prepared by arc melting the pure elements under a purified Ar atmosphere and in situ suction casting in a Cu mold. The amorphous nature of the as-cast alloys was ascertained by x-ray diffraction (XRD), differential scanning calorimetry (DSC) with a heating rate of 20 K/min, transmission electron microscopy (TEM), and high-resolution TEM (HRTEM). Elastic moduli of the BMGs were monitored by means of an ultrasonic method (14). The samples with a gauge aspect ratio of 2:1 were cut out of the as-cast 2-mm rods for uniaxial compression tests.

A family of quaternary ZrCuNiAl BMGs was obtained with the compositions shown in the green area of Fig. 1A. Acoustic measurements show that some compositions, such as $Zr_{61.88}Cu_{18}Ni_{10.12}Al_{10}$, $Zr_{64.13}Cu_{15.75}Ni_{10.12}Al_{10}$, and $Zr_{62}Cu_{15.5}Ni_{12.5}Al_{10}$ (labeled as S1, S2, and S3, respectively), exhibit larger values of ν relative to that of other BMGs in this composition range (Table 1). However, their densities are very similar (Table 1). Figure 1B shows that these BMGs can be cast into entirely glassy rods with diameters up to 5 mm without the observation of any apparent crystalline Bragg peaks. Clear glass transitions and sharp crystallization events are observed in the DSC traces (Fig. 1C), confirming the glassy nature of the BMGs. The thermal parameters are also summarized in Table 1.

Multiple compression tests were performed at room temperature on compositions S1 to

S3. Figure 2A shows the true stress–true strain curve of S2 and those of S1 and S3 are shown in the inset. Similar to other typical BMGs, S1, S2, and S3 exhibit elastic strain limits of $\sim 2\%$ before yielding at 1733, 1690, and 1851 MPa, respectively. However, after yielding, the materials display stress overshoot, as is often observed in superplastic deformation in the supercooled liquid state (15, 16). True strains as large as $\sim 160\%$ were achieved. As a result of such intense deformation, the BMG rods were compressed into flakes (Fig. 2B) without fracturing. The diameter of the flakes is more than 5 mm and could be expanded to larger sizes, implying high flowability of the BMGs. Moreover, the BMGs could be bent into desired shapes (Fig. 2C) similar to flexible metals such as Al and Cu. The maximum bending angle approaches 90° in both rods and plates. Such unusual degrees of plasticity and flexibility were previously obtained for BMGs in a supercooled liquid state at high temperatures (17).

As shown in Fig. 2A, the flow stress of S2 increases with increasing strain after stress overshoot. However, the rapid increase of flow stress (when strain is $>80\%$) is not due to the strain-hardening. We conducted compression tests on S2 and unloaded at different plastic strains. As shown in Fig. 2D, the samples' barrel-like shape implies that friction occurs at the contact surfaces between the sample and the tungsten carbide platens (18). The friction would increase flow stress, especially in the late stage of deformation because of the large increase of transversal area of the specimen and thus the decreased aspect ratio (19). The hardness of the heavily deformed flake is only slightly greater than that of the as-cast sample, suggesting that only negligible strain-hardening occurs. Consistent with previous work (20–22), the deformation of the BMGs also exhibits strain-rate softening and serrated flow behaviors.

Unlike in crystalline metals, dislocation-mediated deformation is not available in BMGs. The formation and evolution of shear bands are the main processes that account for the plasticity of BMGs, especially at low temperatures. Scanning electron microscope (SEM) observations on the specimen surface are given in Fig. 3. Figure 3A shows two important features of shear bands at true plastic strain of 2.7%. First, the

uniform shear bands, including premature shear bands, are formed in different directions even at the initial stage of the plastic deformation. This results from the interaction of the shear bands that alter surrounding stress fields and bring an increased local stress level (23) to compensate the shear band-induced softening (8). The premature bands would carry further plastic strain, avoiding the occurrence of catastrophic failure. Second, the shear bands appear wavy. The periodicity of the wave is about 1 to 3 μm , which is consistent with the size of the hard regions in the glasses. In addition, winglike shear bands were formed along the primary shear bands (black arrows in Fig. 3A) and even along the premature wavy shear bands (white arrows in Fig. 3A, inset). The winglike bands can be extended and linked together to sustain ever-increasing deformation. After true plastic strain of $\sim 160\%$, a high density of shear bands is formed (Fig. 3B). The BMGs have evolved into polycrystal-like patterns with shear bands serving as “grain boundaries.” Nanoscale cracks were also found, but none of them carried enough deformation to cause specimen fracture. The BMGs seem to deform in a

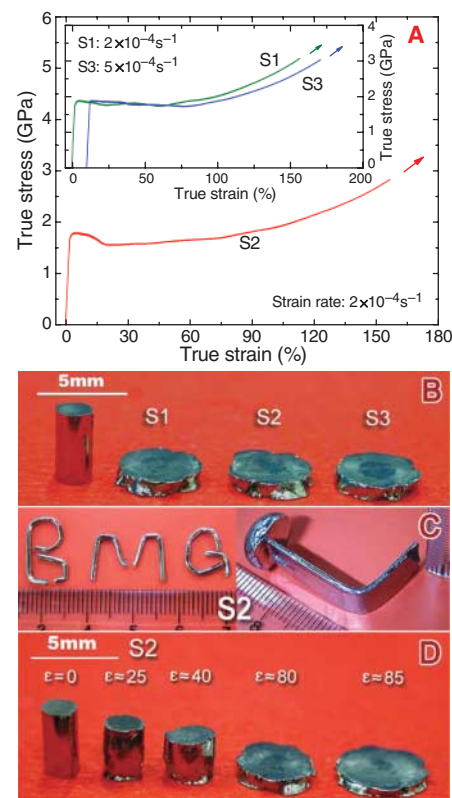


Fig. 2. (A) True stress–true strain curve of S2 tested at room temperature. The inset shows those of S1 and S3. The strain rate imposed is $2 \times 10^{-4} \text{ s}^{-1}$ for S1 and S2 and $5 \times 10^{-4} \text{ s}^{-1}$ for S3, respectively. (B) Compressed flakes of S1, S2, and S3. (C) S2 bent into different shapes, showing exceptional deformability. (D) S2 deformed to various nominal strains. A barrel shape can be seen, which implies that friction between the sample and the platens occurred.

Table 1. Glass transition temperature T_g , crystallization temperature T_x (obtained by DSC at a heating rate of 20 K/min), and elastic constants (E , the shear modulus G , the bulk modulus K , and ν) measured by an ultrasonic method for the super plastic BMGs and a representative BMG (Inoue's ZrCuNiAl BMG) in the green BMG-forming composition range indicated in Fig. 1A are shown. The range of values for ν of the ZrCuNiAl BMGs with poor or limited plasticity in the composition range is from 0.350 to 0.375. ρ , density.

BMG	T_g (K)	T_x (K)	ρ (g/cm^3)	E (GPa)	G (GPa)	K (GPa)	ν
$Zr_{61.88}Cu_{18}Ni_{10.12}Al_{10}$ (S1)	653	744	6.649	80.12	29.10	108.33	0.377
$Zr_{64.13}Cu_{15.75}Ni_{10.12}Al_{10}$ (S2)	643	745	6.604	78.41	28.46	106.63	0.377
$Zr_{62}Cu_{15.5}Ni_{12.5}Al_{10}$ (S3)	652	748	6.615	79.65	28.89	109.03	0.378
Inoue's $Zr_{65}Cu_{15}Ni_{10}Al_{10}$			6.642	82.96	30.27	106.65	0.355

macroscopically near-homogenous manner through profuse and concurrent shear-band formation (8), even though the plastic strain is localized. The case resembles that of crystals, where plastic strain is localized in slip bands.

In order to correlate the extraordinary plasticity of the glasses with their structure, TEM investigations were performed to reveal their microstructural features. Figure 4A shows the bright-field image of the as-cast S2. The most notable characteristic is that the BMG is composed of isolated dark zones, ranging from 2 to 5 μm in size, that are surrounded by continuous bright zones, which are about 0.5 to 1 μm in width. The volume fraction of the bright zones is estimated to be $\sim 10\%$. The strong contrast indicates that the bright zones are thinner than the dark ones, implying a higher thinning rate in the bright zones under the ion beam, which comes from the difference in mass-to-thickness contrast produced by the lower density of the bright zones, where holes even occur (Fig. 4A). Similar microstructures are observed for S1 and S3 (Fig.

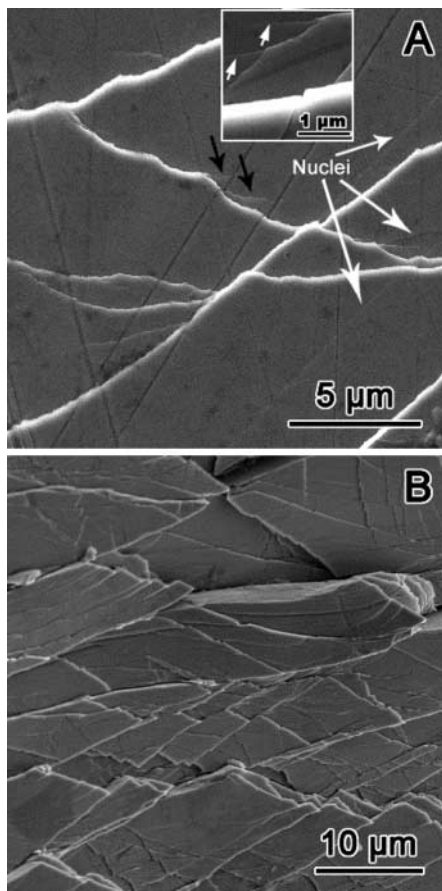
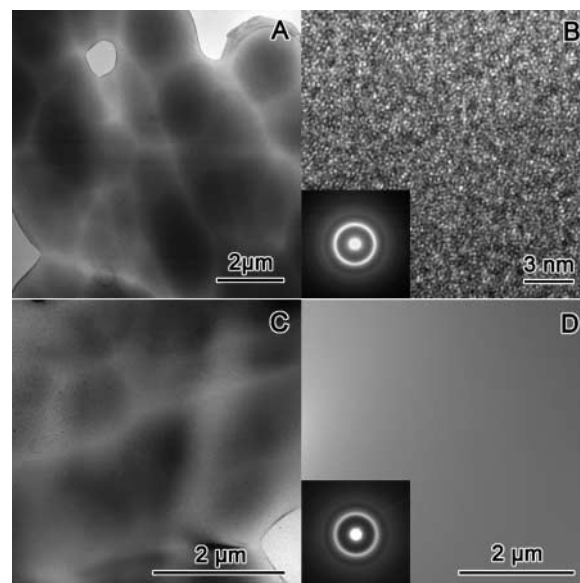


Fig. 3. The SEM images of the surface of the S2 specimen deformed to true plastic strain of $\sim 2.7\%$ (A) and $\sim 159\%$ (B), respectively. The shear bands in (A) appear wavy, and the length of the wave is comparable to that of the dark regions in Fig. 4, (A) and (B). Black arrows indicate winglike shear bands. Nuclei, shear-band nuclei. The inset shows winglike shear bands along the premature wavy ones (arrows).

4C and fig. S1) but cannot be found in a conventional BMG (Fig. 4D), indicating that this is not an artifact from TEM sample preparation. The selected-area electron diffraction (SAED) patterns in both bright and dark zones are halo rings, confirming the glassy nature in both zones. No traces of phase separation, which occurs usually on the nanoscale (3), were observed. The energy-dispersive x-ray analysis did not show any substantial composition variation in both bright and dark zones, excluding the possibility of the occurrence of phase separation (3) (fig. S2). The detailed structure of the bright and dark zones was also examined by means of HRTEM (Fig. 4B). The similar mazelike patterns without any crystalline fringe, which are typical features of glass, can be widely observed. Instrumented nanoindentation tests on the as-cast super plastic BMGs show that a large fluctuation of load is required to penetrate identical depth (500 nm, corresponding to an indentation size of $\sim 4 \mu\text{m}$) (fig. S3), which indicates strength variations in the glasses. The structural studies confirm the chemical and compositional homogeneity and single glassy nature of the BMGs. However, the preferential thinning in the bright zones indicates that the bright zones are softer than the dark zones or that there are much more thermally unstable atomic-scale open volumes existing in the bright zones (24, 25). A similar structural feature has also been found in Pd-based BMGs (26). We suggest a microstructure, composed of hard regions surrounded by soft regions (with larger values of v), in the super plastic BMGs. The slight increase in the fraction of the soft regions would augment v steeply without substantial changes in overall density (26). The relatively large v value of these BMGs, which was determined by an ultrasonic method, is an indicator of the high concentration of such open volumes in the glasses. The question of what gives rise to this distinctive structural feature is a challenging subject for the future.

Fig. 4. (A) TEM image of S2 showing dark regions surrounded by bright regions (corresponding to hard and soft regions, respectively), in which some soft regions were thinned into holes. (B) HRTEM images show mazelike patterns that confirm the glassy nature of the BMGs. The insets in (B) and (D) show SAED patterns. In both dark and bright regions, HRTEM and SAED patterns are identical, implying that no phase separation occurs. Similar structures are also found in S1 (C). However, the structures are not observed in conventionally brittle BMGs, such as $\text{Zr}_{59.63}\text{Cu}_{15.75}\text{Ni}_{14.62}\text{Al}_{10}$ (D).



A possible explanation for the origin of the concurrent and homogeneous formation of copious shear bands, and hence the extreme deformability, is based on the distinctive structure of the BMGs. The shear transformation zones (27), which begin as small regions where the local atomic structure is capable of rearrangement under an applied shear stress, serve as the nucleation sites for the shear bands. The ability of a region to undergo a shear transformation depends on the local microstructure (28). The shear transformation zones occur preferentially in soft regions in BMGs and evolve into shear bands upon loading. Consequently, numerous shear-band nuclei are formed concurrently in the soft regions. However, the shear-band propagation would be impeded by the hard regions. This impedance alters the propagating directions and assists shear-band multiplication, resulting in the wavelike appearance of the shear bands and the formation of wing bands. The interactions between the shear bands and hard regions would compensate the softening induced by their formation (8). The consistency between the wave periodicity of shear bands in Fig. 3A and that of hard regions in Fig. 4 supports the assumption. Because the soft regions cannot carry more plastic strain, further plastic deformation has to proceed in hard regions so that more plasticity is still attainable. These factors imbue the BMGs with super plasticity. HRTEM observations do not reveal nanocrystals even in heavily deformed flakes. This indicates that the super plasticity is not a result from the stress-induced nanocrystallization as found in other BMGs (29); instead, it is an intrinsic property. Annealing of the BMGs below the glass transition temperature dramatically decreases the plasticity, because the annealing can remove thermally unstable atomic-scale open volumes that exist in the soft regions, decreasing the fraction of the soft regions and reducing v (30, 31). On the other hand, the introduction of a high population of preexisting

shear bands can dramatically increase plasticity of BMGs (32). These results confirm that a structural feature is the cause of the super plasticity of the BMGs, and the homogeneous and concurrent formation of multiple shear bands throughout the samples is crucial for the improvement of plasticity in BMGs.

This unusual plasticity can shed light on some fundamental issues on the deformation and fracture of BMGs, such as the dynamics of plastic deformation (5). We measured the evolution of shear-band spacing d with increasing nominal strain ϵ . It was found that d correlates with ϵ via a power-law relation ($d = A\epsilon^{-B}$) where A is a constant and $B = 1.45$, which is different from the value obtained by decreasing the sample's aspect ratio (height/diameter) to less than 1.0 (8).

Similar to the glass-forming ability of BMG-forming alloys (33), the super plasticity of the BMGs is very sensitive to their composition. Minor deviations in content (<1 atomic %) can substantially change the plasticity of the BMGs. The results indicate that, even in the reported BMG systems, extraordinarily plastic BMGs may be obtained by the appropriate choice of their composition with the use of the Poisson's ratio strategy. The present investigation has focused on Zr-based BMGs. We expect that the strategy would provide useful guidelines for the develop-

ment of super plastic BMGs as high-performance structural materials in other known or unknown BMG-forming alloys and open an area of research of both fundamental and applied importance.

References and Notes

- J. Schiötz, K. W. Jacobsen, *Science* **301**, 1357 (2003).
- K. S. Kumar, H. V. Swygenhoven, S. Suresh, *Acta Mater.* **51**, 5743 (2003).
- A. L. Greer, *Science* **267**, 1947 (1995).
- L. Q. Xing, Y. Li, K. T. Ramesh, J. Li, T. C. Hufnagel, *Phys. Rev. B* **64**, 180201 (2001).
- D. M. Dimiduk, C. Woodward, R. LeSar, M. D. Uchic, *Science* **312**, 1188 (2006).
- J. Das et al., *Phys. Rev. Lett.* **94**, 205501 (2005).
- Z. F. Zhang, H. Zhang, X. F. Pan, J. Das, J. Eckert, *Philos. Mag. Lett.* **85**, 513 (2005).
- H. Bei, S. Xie, E. P. George, *Phys. Rev. Lett.* **96**, 105503 (2006).
- J. Schroers, W. L. Johnson, *Phys. Rev. Lett.* **93**, 255506 (2004).
- E. Ma, *Nat. Mater.* **2**, 7 (2003).
- J. J. Lewandowski, W. H. Wang, A. L. Greer, *Philos. Mag. Lett.* **85**, 77 (2005).
- Q. Zheng, H. Ma, E. Ma, J. Xu, *Scripta Mater.* **55**, 541 (2006).
- X. J. Gu, A. G. McDermott, S. J. Poon, G. J. Shiflet, *Appl. Phys. Lett.* **88**, 211905 (2006).
- W. H. Wang, *J. Appl. Phys.* **99**, 093506 (2006).
- J. Lu, G. G. Ravichandran, W. L. Johnson, *Acta Mater.* **51**, 3429 (2003).
- Y. Kawamura, A. Inoue, T. Masumoto, *Appl. Phys. Lett.* **71**, 779 (1997).
- F. Spaepen, *Acta Mater.* **25**, 407 (1977).
- T. El-Aguizy, J. S. Plante, A. H. Slocum, J. K. Vogan, *Rev. Sci. Instrum.* **76**, 075108 (2005).
- M. N. Charalambides, S. M. Goh, L. Wanigasooriya, J. G. Williams, W. Xiao, *J. Mater. Sci.* **40**, 3375 (2005).
- T. Mukai, T. G. Nieh, Y. Yoshihito, A. Inoue, K. Higashi, *Intermetallics* **10**, 1071 (2002).
- T. C. Hufnagel, T. Jiao, Y. Li, K. T. Ramesh, *J. Mater. Res.* **17**, 1441 (2002).
- W. J. Wright, R. Saha, W. D. Nix, *Mater. Trans.* **42**, 642 (2001).
- J. Eckert et al., *Intermetallics* **14**, 876 (2006).
- C. Nagel, K. Rätzke, E. Schmidtke, F. Faupel, W. Ulfert, *Phys. Rev. B* **60**, 9212 (1999).
- D. Suh, R. H. Dauskardt, P. A. Kumar, P. A. Sterne, R. H. Howell, *J. Mater. Res.* **18**, 2021 (2003).
- T. Ichitsubo et al., *Phys. Rev. Lett.* **95**, 245501 (2005).
- A. S. Argon, *Acta Mater.* **27**, 47 (1979).
- B. P. Kanungo, S. C. Glade, P. A. Kumar, K. M. Flores, *Intermetallics* **12**, 1073 (2004).
- M. W. Chen, A. Inoue, W. Zhang, T. Sakurai, *Phys. Rev. Lett.* **96**, 245502 (2006).
- L. M. Wang, W. H. Wang, R. J. Wang, *Appl. Phys. Lett.* **77**, 1147 (2000).
- P. Murali, U. Ramamurty, *Acta Mater.* **53**, 1467 (2005).
- Y. Zhang, W. H. Wang, A. L. Greer, *Nat. Mater.* **5**, 857 (2006).
- D. Wang, H. Tan, Y. Li, *Acta Mater.* **53**, 2969 (2005).
- Financial support is from the NSF of China (grant number 50621061) and the Chinese Academy of Sciences.

Supporting Online Material

www.sciencemag.org/cgi/content/full/315/5817/1385/DC1
Materials and Methods
Figs. S1 to S3
References

25 October 2006; accepted 4 January 2007
10.1126/science.1136726

Quantum Hall Effect in Polar Oxide Heterostructures

A. Tsukazaki,¹ A. Ohtomo,^{1,2*} T. Kita,^{3,4} Y. Ohno,⁴ H. Ohno,^{3,4} M. Kawasaki^{1,5*}

We observed Shubnikov–de Haas oscillation and the quantum Hall effect in a high-mobility two-dimensional electron gas in polar ZnO/Mg_xZn_{1-x}O heterostructures grown by laser molecular beam epitaxy. The electron density could be controlled in a range of 0.7×10^{12} to 3.7×10^{12} per square centimeter by tuning the magnesium content in the barriers and the growth polarity. From the temperature dependence of the oscillation amplitude, the effective mass of the two-dimensional electrons was derived as 0.32 ± 0.03 times the free electron mass. Demonstration of the quantum Hall effect in an oxide heterostructure presents the possibility of combining quantum Hall physics with the versatile functionality of metal oxides in complex heterostructures.

Zinc oxide (ZnO), a wide-band gap semiconductor, is of growing importance in advanced electronics, and its potential applications include transparent conducting oxide layers for flat-panel displays and transparent

field-effect transistors (1). Research focused on the epitaxial growth of ZnO, particularly in terms of its novel excitonic properties, has led to the recent realization of homostructural light-emitting diodes (2). Studies of the intrinsic properties of ZnO have yielded a recipe for the preparation of high-quality epilayers having high mobility and excitonic luminescence with high quantum efficiency (3, 4).

Certain aspects of two-dimensional electron gas (2DEG) behavior in semiconductor heterostructures have been studied by observing the quantum Hall effect (QHE)—a quantized magnetotransport accompanied by Shubnikov–de Haas (SdH) oscillations in the longitudinal resistivity ρ_{xx} and Landau plateaus in the Hall

resistivity ρ_{xy} (5). Early results were obtained in the material systems of Si/SiO₂ or GaAs/AlGaAs (6, 7). However, after discovery of the fractional QHE (8, 9), the focus has been extended to a variety of other material systems, such as III-nitrides (10) and graphene (11). The observation of SdH oscillation requires conditions such as $\omega_c\tau > 1$ and $\hbar\omega_c > k_B T$, where ω_c is the cyclotron frequency equal to eB/m^* (where e is the charge on the electron, B is magnetic field, and m^* is the electron effective mass), τ is the carrier relaxation time, \hbar is Planck's constant divided by 2π , k_B is Boltzmann's constant, and T is absolute temperature. Although several epitaxial oxide heterostructures have satisfied these conditions (12), the QHE has not been observed in those materials. [However, a QHE-like state was seen in a quasi-2D crystal of bulk η -Mo₄O₁₄ (13).]

In our study, (0001)-oriented ZnO/Mg_xZn_{1-x}O heterostructures were grown by laser molecular beam epitaxy with the use of a semiconductor-laser heating system (3). The Mg_xZn_{1-x}O layer acts as a potential barrier for the 2DEG in the adjacent ZnO layer (14). We used a temperature gradient method that allowed us to grow the films over a wide range of temperatures on a single substrate (3). The three samples (samples A, B, and C) discussed here were of such high quality that we were able to look at the effects of growth temperature (T_g) of the ZnO layers and Mg content x in the barrier layers (Table 1) [see (15) for sample preparation and characterizations]. Sample A was selected from the highest- T_g region

¹Institute for Materials Research, Tohoku University, Sendai 980-8577, Japan. ²PRESTO, Japan Science and Technology Agency, Kawaguchi 332-0012, Japan. ³ERATO Semiconductor Spintronics Project, Japan Science and Technology Agency, Sendai 980-0023, Japan. ⁴Laboratory for Nanoelectronics and Spintronics, Research Institute of Electrical Communication, Tohoku University, Sendai 980-8577, Japan. ⁵CREST, Japan Science and Technology Agency, Kawaguchi 332-0012, Japan.

*To whom correspondence should be addressed. E-mail: aotomo@imr.tohoku.ac.jp (A.O.); kawasaki@imr.tohoku.ac.jp (M.K.)